Available online at www.sciencedirect.com
SCIENCE DIRECT®
Solid-State Electronics 49 (2005) 535–544
SOLID-STATE ELECTRONICS
www.elsevier.com/locate/sse

Physical study of the avalanche breakdown phenomenon in HEMTs

M. Elkhou *, M. Rousseau, H. Gerard, J.C. De Jaeger

Institut d'Electronique, de Microélectronique et de Nanotechnologie Cité scientifique, Av Poincaré, BP 69, 59652 Villeneuve d'Ascq, France

Received 23 February 2004; received in revised form 20 December 2004; accepted 1 January 2005

The review of this paper was arranged by Prof. S. Cristoloveanu

Abstract

The aim of this study is the physical understanding of the avalanche breakdown phenomenon in PHEMTs (AlGaAs/GaInAs/GaAs), in order to optimise the structure and to improve the breakdown voltage. It is therefore necessary to study the influence of the physical parameters on which this phenomenon depends, such as the layer structure, the doping concentration or the gate recess topology. The study is based on a two-dimensional hydrodynamic modelling, that takes electrons and holes into account, and shows that the highest breakdown voltage is obtained for a double step gate recess with two delta-doping layer plans.

Keywords: Hydrodynamic modelling; Pseudomorphic HEMTs; Single and double step gate recess; Avalanche breakdown phenomenon

1. Introduction

A lot of progress has been made concerning the performance of High Electron Mobility Transistors (HEMTs) [1–4]. However, the avalanche breakdown phenomenon constitutes one of the main limitations of this component for microwave power amplification. Thus, the physical understanding of this phenomenon is essential for studying and improving the breakdown voltage. For our purposes, it is necessary to analyse the influence of all the physical parameters implied in this phenomenon, such as the delta doping plans and the gate recess topology. We have used the hydrodynamic model, which has been described by several authors [3,4] because it can provide accurate results with a reasonable computational cost. Thus it is a good way to optimise a component and to reduce the manufacturing cost. This model is obtained from the Boltzmann's transport equation using the method of the moments. A set of conservation equations for the following macroscopic average quantities is obtained: electrons and holes velocities, carrier density and energy of the electrons.

The focus of this paper is on the avalanche breakdown phenomenon analysis. In Section 2, a generalised hydrodynamic model, which includes the avalanche breakdown phenomenon in the channel, is presented. Indeed, the minority carriers and the generation and recombination terms are taken into account in the conservation equations. In Section 3, the AlGaAs/GaInAs/GaAs pseudomorphic HEMT with single step gate recess and two delta-doped layers is studied: First, the experimental and theoretical I_{DS} (V_{DS}, V_{GS}) characteristics are compared. Then, the physical quantities are analysed. In Section 3.3, the structures with one or two delta-doped layers are compared, and in Section 3.4, the influence of the gate recess is studied.

* Corresponding author. Tel.: +333 20 19 78 93/336 11 18 22 56; fax: +333 20 19 78 88.
E-mail address: majda.elkhou@iemn.univ-lille1.fr (M. Elkhou).

0038-1101/$ - see front matter © 2005 Elsevier Ltd. All rights reserved.
doi:10.1016/j.sse.2005.01.003

Nomenclature

n	electron concentration	κ	thermal conductivity
n_i	intrinsic concentration	w	carrier energy
p	hole concentration	$\varepsilon_0\varepsilon_r$	dielectric permittivity
$\lvert\vec{v}_n\rvert$	electron average drift velocity	V_B	Schottky barrier height
$\lvert\vec{v}_p\rvert$	hole average drift velocity	m^*	effective mass
R	recombination rate	E_0	electric field in the spacer
G	generation rate	q	electron charge
α_n	electrons ionisation coefficient	N_d^+	ionised impurities concentration
α_p	holes ionisation coefficient	μ_n	electron mobility
w_p	optical phonon energy	μ_p	hole mobility
k_B	Boltzmann's constant	λ_0	asymptotic value of the mean free path at high energy and low temperature
T_e	electronic temperature		
T_0	lattice temperature		

2. Model description

The numerical model is based on the conservation equations of semiconductors deduced from Boltzmann's equation and coupled with Poisson's equation.

The introduction of the avalanche breakdown phenomenon in the two-dimensional (2D) hydrodynamic model requires taking into account minority carriers and generation and recombination terms.

2.1. Basic equations

Continuity equations for electrons or holes:

$$\frac{\partial n}{\partial t} + \operatorname{div}(n\vec{v}_n) = G - R \tag{1a}$$

and

$$\frac{\partial p}{\partial t} + \operatorname{div}(p\vec{v}_p) = G - R \tag{1b}$$

In these equations, the band to band recombination rate R is modelled by using the following expression:

$$R = k(np - n_i^2) \tag{1c}$$

where n_i is the intrinsic carrier concentration and the constant k is 2×10^{-16} m^3/s [5].

The generation rate G is given by

$$G = \alpha_n n|\vec{v}_n| + \alpha_p p|\vec{v}_p| \tag{1d}$$

The ionisation coefficients, α_n for the electrons and α_p for the holes, are defined as the number of electron–hole pairs created by carrier and by unit of length in the direction of the applied electric field. They are given by the following equation [6]:

$$\alpha_{n,p}(E) = \frac{qE}{w_i}\exp(A - \sqrt{A^2 + X^2}) \tag{1e}$$

w_i is the ionisation threshold energy at high field, E is the electric field, A and X are given by the following equations:

$$A = 0.217\left[\frac{w_i}{\langle w_p\rangle}\right]^{1.14} \quad \text{and} \quad X = \frac{w_i}{qE\lambda}$$

with

$$\lambda = \lambda_0 \tanh\frac{w_p}{2k_BT_e} \quad \text{and} \quad \langle w_p\rangle = w_p \tanh\frac{w_p}{2k_BT_e}$$

w_p is the energy of the optical phonons, λ_0 is the asymptotic value of the mean free path at high energy and low temperature, k_B is the Boltzmann's constant and T_e is the electronic temperature.

An electron submitted to an electric field is not able to generate ionisation phenomenon if its energy is lower than a threshold level. It must drift on a certain length called black space, where there is a strong electric field, before being able to ionise. To take these effects into account, the electron ionisation coefficient is expressed as a function of the average electron energy, by using the relation between the electric field and the average energy obtained from Monte-Carlo simulation in bulk. However, the usual Monte-Carlo model is limited to electric fields close to 5×10^6 V/m, whereas the breakdown effects occur for a higher electric field. To avoid this problem, it is necessary to use the Monte-Carlo model giving the transport properties of materials when strong fields are considered [7]. With this model, it is possible to determine the energy evolution according to electric fields up to 150×10^6 V/m.

Energy conservation equation:

$$\frac{\partial nw}{\partial t} = -qn\vec{v}\vec{E} - \nabla\vec{S}_n - \frac{n(w - w_0)}{\tau_w} - w\cdot(G - R) \tag{2a}$$

$\vec{S}_n$ is the energy flow for electrons, given by

$$\vec{S}_n = \vec{Q}_n + [w + k_BT_e(w)]n\vec{v} \tag{2b}$$

where the heat flux $\vec{Q}_n$ is given by the Wiedeman Frantz law [8]:

$$\vec{Q}_n = -\kappa \nabla \vec{T}_e \tag{2c}$$

and κ is the thermal conductivity of the considered carrier gas, given by

$$\kappa = \left(\frac{5}{2} + c\right)\left(\frac{k_B}{q}\right)^2 qn\mu T_e \tag{2d}$$

The hole energy conservation equation is not taken into account in our model because of the bad transport properties of holes, which give a low energy gain. A drift diffusion model is used for these minority carriers.

Velocity equations for electrons and holes:

$$\vec{v}_n = \mu_n\left[-\vec{E} - \frac{1}{n}\vec{\nabla}(nk_B T_e)\right] \tag{3a}$$

and

$$\vec{v}_p = \mu_p\left[\vec{E} - \frac{1}{p}\vec{\nabla}(pk_B T_0)\right] \tag{3b}$$

These equations are the simplified form of the moment equation, obtained by neglecting the inertial terms [9].

Poisson's equation:

$$\nabla(\varepsilon_0 \varepsilon_r \vec{E}) = q(N_d^+ - n + p) \tag{4}$$

The evolutions of T_e, μ_n, μ_p and τ_w with energy are obtained from a three valleys Monte-Carlo bulk simulation in stationary regime [10]. The transport properties of the strained GaInAs are those of the GaAs.

2.2. Numerical resolution

In order to reduce the high computing time, resulting from the large number of equations to be solved, the component active part only is simulated. This restriction of the simulated area leads to establish the following boundary conditions: Dirichlet's boundary conditions on the source and drain electrodes ($T_e = T_0$, $n = N_d^+$, $V = V_{source}$ or V_{drain}) and Neumann's boundary conditions on the free surfaces, in order to keep currents across these surfaces equal to zero. On the gate, the Schottky contact is supposed to be ideal, with a barrier height equal to V_B. Therefore, the gate potential is $V = V_{GS} + V_B$, where V_{GS} is the applied potential.

To take the conduction band and the valence band discontinuities into account, the following treatment is used:

- At the interface corresponding to the node i_I, the thermionic current density is used:

$$J_y = -q\left[v_2(T_2)\cdot n_2 - \frac{m_2^*}{m_1^*}\cdot v_1(T_1)\cdot n_1 \cdot \exp\left[-\frac{\Delta E_c}{k_B T_1}\right]\right] \tag{5}$$

where m_1^* and m_2^* are the electron effective masses in the small and in the large gap semiconductors, respectively, and T_1, T_2 are their respective electronic temperatures.

- At the dots i_{I-1}, i_{I-2}, i_{I-3} and i_{I-4}, the tunnel current density and the drift diffusion current density are used. The tunnel current is given by

$$J_{TUN_i} = -q\left[\left(n_{i_{I-h,j}} v_{2_{I-h}} - n_{i_{I-h+1,j}} v_{2_{I-h+1}}\right) - \frac{n_{i_{I+h,j}} v_{1_{I+h}}}{m^*_{1_{I+h}}} \exp\left(-\frac{\Delta E_c}{kT}\right)\left(m^*_{2_{I-h}} \exp\left(\frac{\delta E_h}{k_B T_1}\right) - m^*_{2_{I-h+1}} \exp\left(\frac{\delta E_{h-1}}{k_B T_1}\right)\right)\right] \times P_{TUN_i} \tag{6}$$

where $h \in \{1, 2, 3, 4\}$ and P_{TUN} is the tunnelling probability given for a triangular barrier by

$$P_{TUN_i} = \exp\left[-\frac{4}{3}\left(\frac{2m^* q}{\hbar^2}\right)^{1/2}\frac{\delta E_i^{3/2}}{E_0}\right] \tag{6a}$$

δE_i (eV) is the energy difference between the node "i" and the interface.

The surface potential is modelled by introducing fixed charges around the gate recess and on the top of the component.

These equations are discretised with a finite difference method where the variables are the potential, V, the electron concentration, n, the hole concentration, p and the electron energy, w. The grid used is non-uniform in the two directions. Poisson's equation is discretised by using a finite-difference method and solved by a double sweep matricial method [11]. The spatial discretisation is achieved by using a centered finite difference method for the conservation equations, and an upwind finite difference method for the current equations. These non-linear equations are linearised by the Newton–Raphson method and solved by a BiCGSTAB algorithm [12] or by an iterative overrelaxation method [13]. The transient regime is simulated until the equilibrium state is reached. This model enables us to obtain the distribution of the physical quantities in the device and the $I(V)$ output characteristics as well as the main elements of the small signal equivalent circuit [14]. It must be mentioned that this paper only deals with the on-state breakdown phenomenon because the gate current determination under reverse bias is not enough accurate due to numerical noise. Consequently the off-state breakdown could not be accurately predicted.

3. Simulation results and discussion

3.1. Ionisation coefficients

The ionisation coefficients of the strained GaInAs and AlGaAs materials, given by the expression (1e),

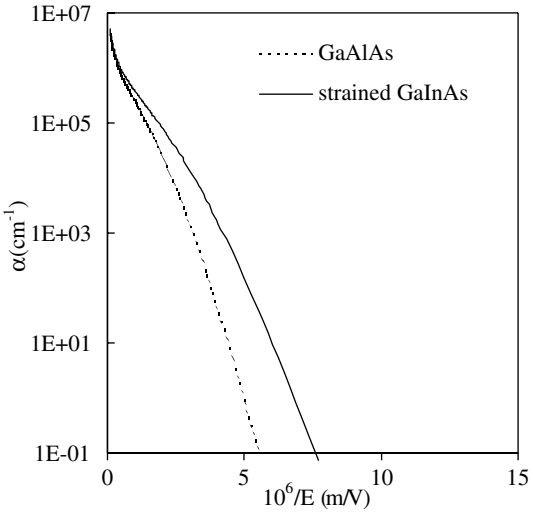

Fig. 1. Strained InGaAs and GaAlAs ionisation coefficient rates versus the electric field reverse.

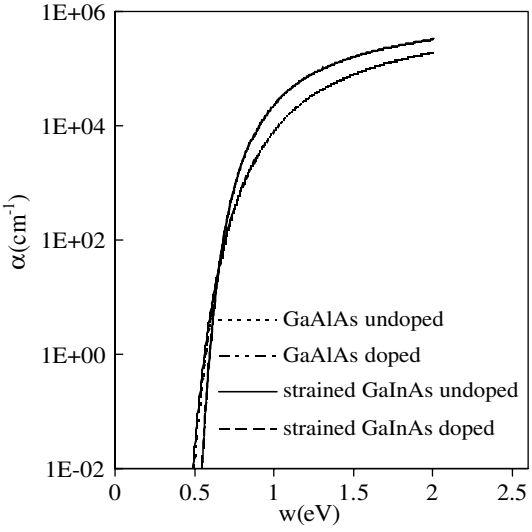

Fig. 2. GaAs and GaAlAs ionisation coefficient rates versus the carrier energy.

are represented versus the reverse electric field in Fig. 1. We can note that the ionisation coefficient is more significant in the material, which has a lower bandgap width. By using the electric field-energy relation, obtained thanks to a Monte-Carlo simulation, the evolution of the ionisation coefficient of GaInAs and GaAlAs versus energy can be deduced (Fig. 2). Results show that the ionisation appears when the value of energy is higher than 0.5 eV in the strained GaInAs and 0.55 eV in AlGaAs materials.

3.2. The basic structure study

In this section, the study deals with the basic structure: AlGaAs/InGaAs/GaAs pseudomorphic HEMT with single step gate recess and two delta-doped layers: First, the topology and the layer structure are presented, then the experimental and theoretical $I_D(V_{DS}, I_{GS})$ characteristics are compared and finally the physical quantities are analysed.

3.2.1. Structure and topology

The studied structure consists of a 100 nm undoped GaAs buffer layer, a 2 nm undoped AlGaAs lower spacer layer, a 2 nm lower delta doped GaAs layer, a 12.2 nm undoped $Ga_{0.78}In_{0.22}As$ channel layer, a 2 nm undoped AlGaAs upper spacer layer, a 3 nm upper delta doped GaAs layer, a 15 nm undoped AlGaAs barrier layer and finally, a 60 nm GaAs cap layer where the source and drain electrodes are deposited. It is a single step gate recess device where the gate recess width is 0.16 μm. The drain–gate distance is 0.75 μm and the gate length is 0.47 μm. The schematic cross section of this structure is shown in Fig. 3.

3.2.2. Comparison with measurements

In order to validate the hydrodynamic model used, it appeared very useful to compare the theoretical predictions with the experimental results.

3.2.2.1. Measurement conditions. The measured transistor is a pseudomorphic HEMT, which has the same structure as the simulated transistor. The topology is $4 \times 50 \times 0.47\ \mu m^2$. The experimental drain–current characteristics versus the drain–source bias for several gate source biases is carried out from a pulsed measurement at a quiescent bias point of $V_{GS0} = 0$ V and $V_{DS0} = 0$ V. This method enables us to eliminate the thermal effects and allows much more important excursions for the drain source and gate source voltages, than in a static

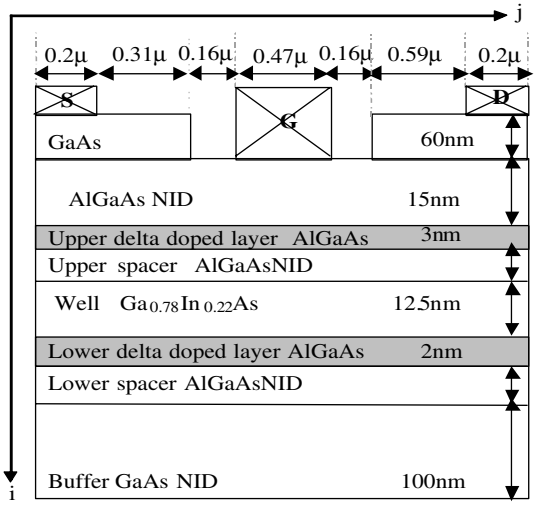

Fig. 3. Schematic cross section of the basic structure studied: AlGaAs/GaInAs/GaAs pseudomorphic HEMT with single step gate recess and two delta-doped layers.

mode. This kind of measure enables us to highlight the increase of current in the I_{DS} (V_{DS}, V_{GS}) characteristics, and to compare the simulated characteristic with the experimental one.

3.2.2.2. $I_D(V_{DS})$ characteristics. The comparison between the simulated and experimental drain–current versus drain source voltage characteristics (Fig. 4) for the previously described structure, shows that the experimental results fit well agreement with the theoretical results because no fitting parameter was used in the simulation. However, the channel conductance gd is lower for the simulated results, due to the doping density in the buffer, which is about 10^{14} cm^{-3} in the simulated structure whereas it is certainly higher in the experimental structure. In order to compare the breakdown voltage resulting from the two determinations, it is necessary to define the theoretical method we used. For a given gate polarisation, the breakdown voltage is usually defined as the value of the V_{DS} voltage for which the gate current reaches the maximum value of 1 mA/mm. It can also be defined as the value of V_{DS} for which the concentration of holes represents 10% of the electron population. In the context of our study, the definition of the breakdown voltage is based on the increase of I_{DS} with V_{DS}. The selected definition supposes that the breakdown voltage is the value of the V_{DS} voltage for which the I_{DS} current exceeds by 10% the value it would have without taking the ionisation phenomena into account [15]. Using this definition, the theoretical breakdown is about 6 V and the experimental one is 5.5 V.

The physical quantities are then analysed with a drain source voltage of 10 V. This bias is chosen because the avalanche breakdown phenomenon is well established in this condition.

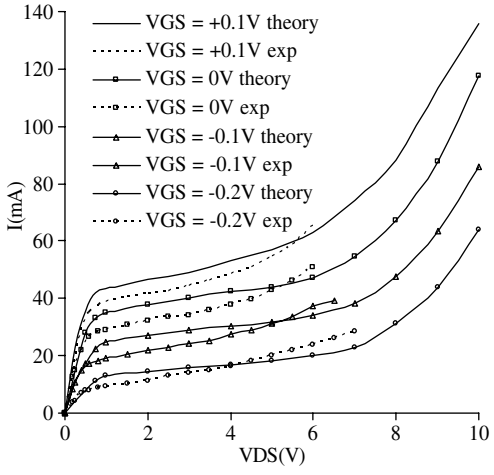

Fig. 4. Comparison between the experimental results and the calculated $I_{DS}(V_{DS}, V_{GS})$ characteristics for single step gate recess structure.

3.2.3. Physical quantities analysis

The average distributions of the physical quantities in the device such as the carrier energy, the generation rate, the electron and hole densities as well as the electron velocity, are compared along the longitudinal axis, with and without generation. These average values are determined in the channel. The transistor biases are the following ones: V_{GS} = +0.2 V and V_{DS} = 10 V.

The longitudinal evolutions of the generation rate and electron energy with and without generation are shown in Fig. 5. It can be noted that the electron–hole generation involves an energy decrease. The maximum energy without generation is 1.47 eV whereas it falls to 1.22 eV when the carrier generation is taken into account while it moves towards the drain. This drop is equal to 18% and is due to the loss of energy when electron–hole carriers are created by avalanche phenomenon. This is modelled by the term $(-w \cdot G)$ added in the energy conservation equation described in Section 2. It can be also noticed that the maximum generation takes place under the gate step recess offset and its value is about 10^{30} cm^{-3}/s. It can be remarked that the maximum of the generation rate precedes the maximum carrier energy. The generation rate peak is narrower than the energy one. This clearly shows that the generation does not only depend on the energy, but also on the current ($n \cdot v$) as established in Eq. (1d).

The carrier density evolutions for electrons and holes in the well are shown in Fig. 6. The average electron density increases with the generation. Under the gate recess, in the area where the generation is maximum, the density increases quickly until it reaches its

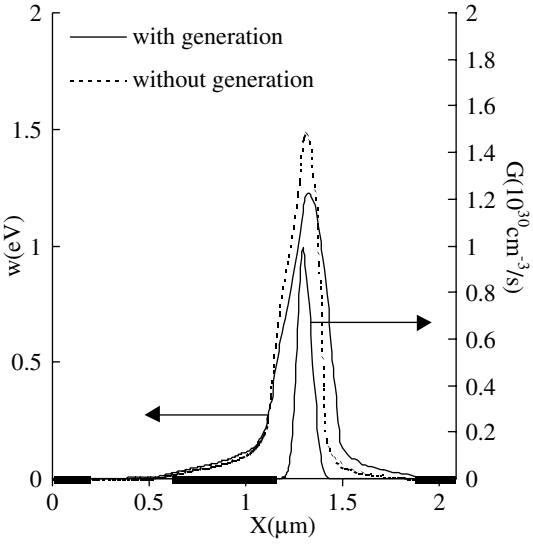

Fig. 5. Average electron energy and generation rate distribution in the channel along the longitudinal axis for a AlGaAs/InGaAs/GaAs PHEMT with a single step gate recess structure, with and without generation. The applied voltages are V_{DS} = 10 V and V_{GS} = +0.2 V.

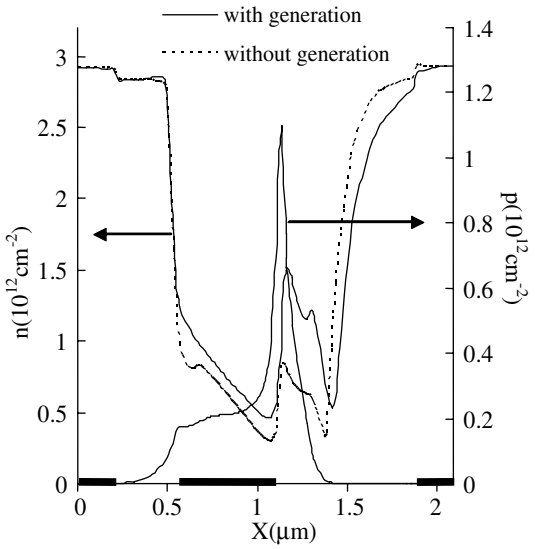

Fig. 6. Average electron and hole density distributions in the channel along the longitudinal axis for a AlGaAs/InGaAs/GaAs PHEMT with a single step gate recess, with and without generation. The applied voltages are V_{DS} = 10 V and V_{GS} = +0.2 V.

maximum, which is $1.46 \times 10^{12}\,cm^{-2}$ as compared to $0.8 \times 10^{12}\,cm^{-2}$ without generation. The hole concentration profile shows a maximum value close to $1.1 \times 10^{12}\,cm^{-2}$, located on the left-hand side of the generation peak. It can also be noted that the gate collects a part of the holes whereas the other part moves towards the source.

After studying the generation influence on the energy and the carrier densities, the electron velocity is analysed (Fig. 7). It shows that under the gate, except at the gate exit, the velocity is higher when the generation phenomenon is taken into account. This is due to a larger longitudinal electric field (E_x) in this area. It is about 4 kV/cm at the gate input instead of 3 kV/cm without carrier generation. This leads to a higher overshoot velocity effect. At the gate exit, the carrier velocity becomes lower, as well as the carrier generation. It is due to a drop in the electric field in this area when the avalanche phenomenon occurs. The carrier velocity has a maximum of 6.3×10^7 cm/s without generation and 5.43×10^7 cm/s with generation.

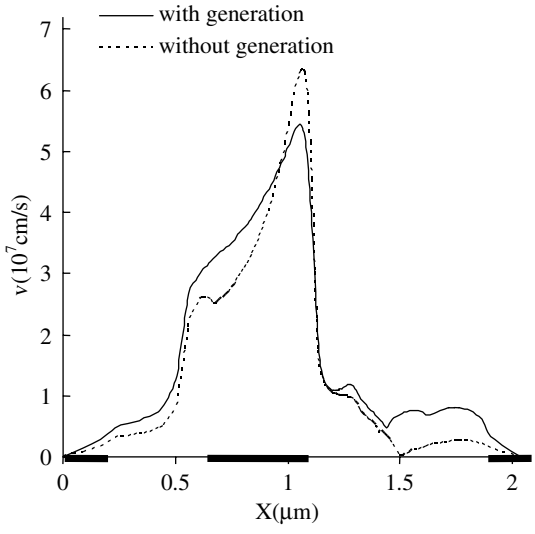

Fig. 7. Electron velocity evolution in the channel along the longitudinal axis for a AlGaAs/InGaAs/GaAs PHEMT with a single step gate recess, with and without generation. The applied voltages are V_{DS} = 10 V and V_{GS} = +0.2 V.

3.3. Delta-doped layers influence

We now compare two different ways of introducing the doping impurities in the structure, in order to improve the pseudomorphic HEMT's power capabilities. It has already been shown that the making of two delta-doping plans makes it possible to obtain strong carriers density in the channel, because the structure presents a double AlGaAs/GaInAs heterojunction. However, this increase involves a drop in the gate-drain breakdown voltage. To study this effect and analyse the delta doped layers influence on the generation, a comparative study of structures having one or two delta-doping plans has been carried out. The studied structures have a single step gate recess and one or two delta-doping layers.

The structure with two delta-doping layers is similar to the structure studied previously. The upper delta doped layer has an active doping concentration of $3 \times 10^{12}\,cm^{-2}$ with a thickness of 3 nm, and the lower delta doped layer has an active doping of $10^{12}\,cm^{-2}$ with a thickness of 2 nm. For the structure with only one delta layer, a doping of $4 \times 10^{12}\,cm^{-2}$, with a thickness of 3 nm, is considered. This doping is equivalent to the total doping of the two delta layers.

This study has been done for a gate source voltage of +0.5 V. This bias has been chosen to provide enough current in the structure with one delta-doped layer because the device is normally off and the pinching voltage is therefore low.

3.3.1. Influence on the energy and the generation rate

Evolutions of the average energy and of the generation rate corresponding to the two structures are represented in Fig. 8. These curves clearly show that the average energy drops for the structure with two delta-doping plans and that it spreads towards the drain by keeping a maximum under the gate step recess offset. As regards the generation rate, it is larger for this last structure. Indeed, its maximum value is $1.1 \times 10^{30}\,cm^{-3}/s$ whereas it is $1 \times 10^{30}\,cm^{-3}/s$ for the structure with one delta doping. This increase (10%) involves the energy drop because of the term $(-w \cdot G)$ in the energy equation, which leads to a lower ionisation coefficient of electrons.

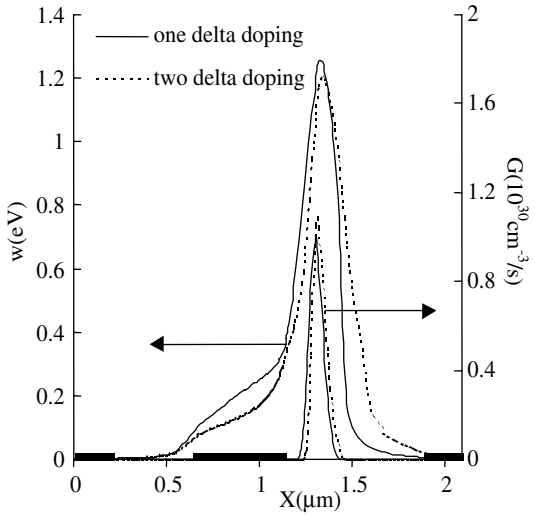

Fig. 8. Average electron energy and generation rate in the channel along the longitudinal axis for a single step gate recess structure with one or two delta-doped layers. The applied voltages are V_{DS} = 10 V and V_{GS} = +0.5 V.

3.3.2. Influence on the minority carriers

According to the above results, the generation is more important with a two delta-doping plan structure. However, the evolution of the minority carriers in the well for the two structures (Fig. 9), shows that the hole concentration for the structure with one delta layer is higher. It also shows that the maximum for this structure is located under the gate, while the maximum corresponding to the structure with only one delta-doping plan shifts towards the source. The study of the hole evolution in the barrier layer (Fig. 9), shows that the hole concentration is higher for the structure with two delta-doping plans than for the one with a single delta plan. This can be explained by the fact that the transverse electric field "E_y" for this structure is larger under the gate. It is more efficient to collect holes.

The structure with two delta-doping plans makes it possible to have a strong carrier density, and consequently a larger current. However, the generation increases by 10% compared with the structure having one delta doped plan, involving a light reduction in the breakdown voltage. The most important risk is an excessive gate current due to the hole concentration increase at the gate exit for this structure. The behaviour of the device will be improved with a higher barrier for the holes.

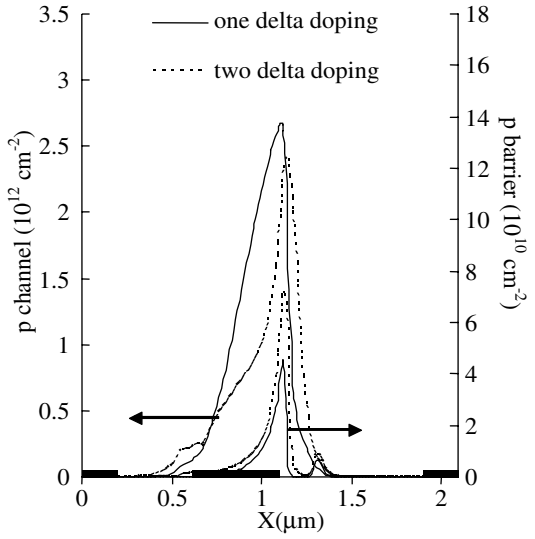

Fig. 9. Average hole densities in the channel and in the barrier layer versus the longitudinal axis for a single step gate recess structure with one or two delta-doped layers. The applied voltages are V_{DS} = 10 V and V_{GS} = +0.5 V.

3.4. Gate recess influence

Experimental results [16–19] have shown that reducing the influence of the breakdown avalanche phenomenon is possible thanks to the use of an adapted profile of the areas located between the gate and drain electrodes. Consequently, we studied two gate-recess topologies: a single step recess and a double step recess. With the help of our model, we compared the results obtained with the two geometries in order to deduce the structure having the highest breakdown voltage.

3.4.1. Double step gate recess structure

The epitaxial layers are the same as the ones of the single step gate recess structure with two delta-doped layers. The length of the narrow gate recess step is 0.16 µm (equal to the length for the structure with a single step gate recess) and the length of the wide one is

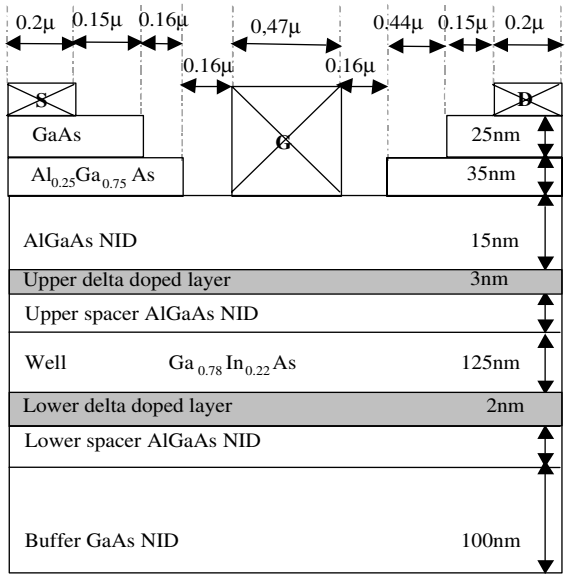

Fig. 10. Schematic cross section for a AlGaAs/InGaAs/GaAs PHEMT with a double step gate recess and two delta-doped layers.

0.44 μm. The thickness of the various layers, the materials used as well as the distances between the electrodes and the gate length are given in Fig. 10.

3.4.2. Influence on the energy and the generation rate

The longitudinal evolutions of the carrier energy and the generation rate at V_{GS} = +0.2 V and V_{DS} = 10 V are represented in Fig. 11. We can observe that the average energy in the well is more important for the structures with a single step gate recess. The maximum is equal to 1.22 eV for this structure, and it is 1.16 eV for the double step recess devices. Under the ionisation threshold (0.5 eV), determined from Fig. 2, the average energy in the structure with a double recess spreads towards the drain while keeping a maximum located under the first step recess. The generation rate is twice lower in the structure with a double step recess involving a larger breakdown voltage. This drop is related to the carrier energy increase and to the product ($n \cdot v$), which is lower.

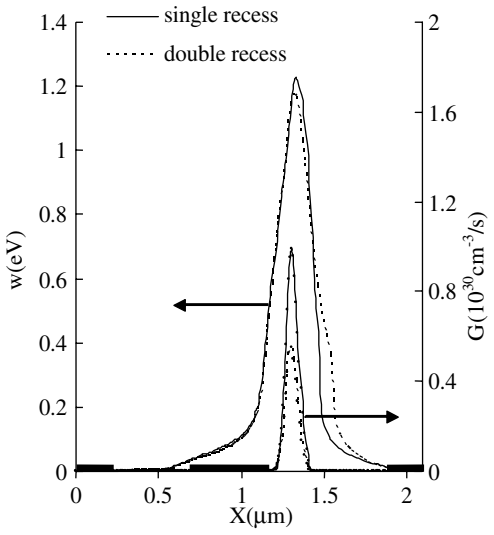

Fig. 11. Average electron energy and generation rate in the channel along the longitudinal axis for a AlGaAs/InGaAs/GaAs PHEMT with a single or a double step gate recess. The applied voltages are V_{DS} = 10 V and V_{GS} = +0.2 V.

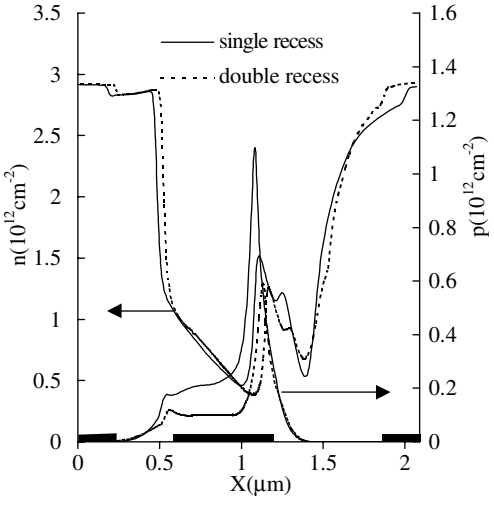

Fig. 12. Average electron and hole densities in the channel along the longitudinal axis for a AlGaAs/InGaAs/GaAs PHEMT with single or a double step gate recess. The applied voltages are V_{DS} = 10 V and V_{GS} = +0.2 V.

3.4.3. Influence on the carrier densities

The majority carrier evolutions of the two structures (Fig. 12) show a strong decrease of the carrier concentration (electrons and holes) for the double step gate recess structure. For the holes, this decrease is due to the generation drop with a factor two. Indeed, the maximum density of holes is about 1.09×10^{12} cm^{-2} for the single step gate recess devices whereas it is 0.6×10^{12} cm^{-2} for the double step gate recess structure.

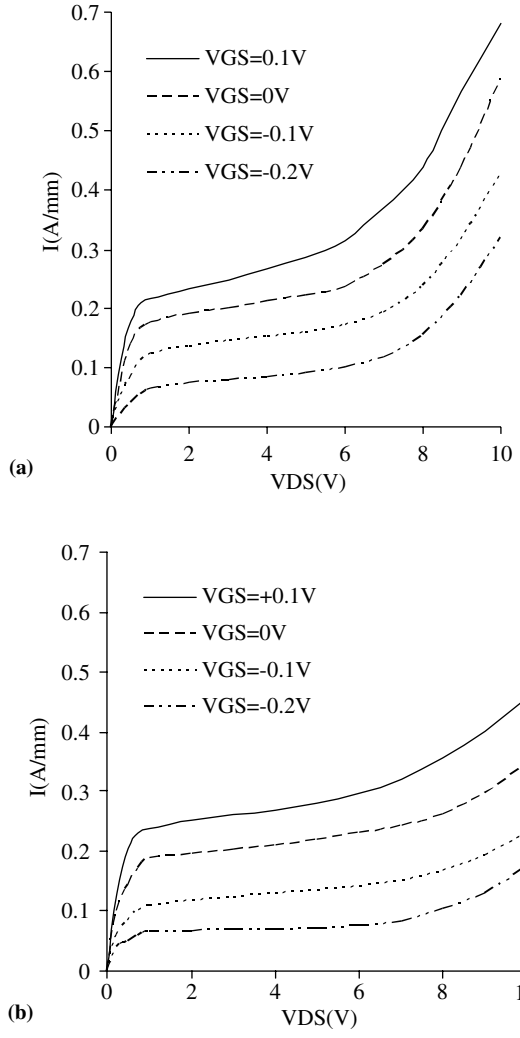

Fig. 13. Dependence of the drain current versus the drain source voltages at different gate voltages for a AlGaAs/InGaAs/GaAs PHEMT with a single (a) or a double step gate recess (b).

3.4.4. $I_D(V_{DS})$ Characteristic comparison

The evolutions of the drain current I_{DS} versus V_{DS} for different gate bias voltages, for the structure with a single or a double step gate recess, are represented in Fig. 13. It is clearly shown that I_{DS} is slightly smaller in the structure with a double step gate recess. For example, for V_{DS} = 6 V and V_{GS} = +0.1 V, this decrease is estimated to 15%. This is due to the surface potential existing in the gate drain space. Comparing the breakdown voltage of the two structures for various V_{GS} biases, it can be observed that the double step gate recess presents a higher breakdown voltage because the carrier generation is divided by a factor two. This breakdown voltage is around 6 V for the structure with the single step gate recess whereas it is around 8 V for the double step recess device. In order to optimise the gate recess, it was shown [14] that digging the second recess up to the drain leads to the best conditions as far as the breakdown is concerned, with a negligible current drop.

4. Conclusion

The avalanche breakdown phenomenon in AlGaAs/InGaAs/GaAs pseudomorphic HEMTs has been studied using the 2D hydrodynamic model. Its validation is carried out by a comparison between the simulated results and the experimental ones.

The generation influence involves the carrier energy drop and this generation rate does not only depend on the energy but also on the current ($n \cdot v$). The analysis of the structures with a single step gate recess with one and two delta-doping plans shows that it is possible to have a strong carrier density in this last structure with a small decrease in the generation rate (10%). However, because of the excessive gate current due to an increase of the hole concentration in the barrier layer, it is necessary to incorporate a high barrier for holes. The comparison between the structures with a single or a double step gate recess with two delta-doping layers shows that the breakdown voltage is strongly related to the gate recess topology. Indeed, it appears that a double step gate recess device gives the highest breakdown voltage. This confirms that this topology is the best one for power field-effect transistors.

Thus, the 2D hydrodynamic model constitutes a useful tool for the optimisation of the avalanche breakdown voltage taking into account realistic topologies of single or double step gate recess. Because of the significant number of technological parameters and the complexity of the device, such a model constitutes a particularly useful tool for the transistor designer in order to reduce the development costs despite the large computing time due to the model complexity.

Acknowledgment

All the simulations have been carried out with the computing facilities of IDRIS (Institut du Développement des Ressources en Informatique Scientifique), Orsay, France, which is to be gratefully acknowledged.

References

[1] Rosenberg JJ, Benlamri M, Kirchner PD, Woodall JM, Pettit GD. An $In_{0.15}Ga_{0.85}As$/GaA pseudomorphic single quantum well HEMT. IEEE Electron Device Lett 1985;6:491–3.
[2] Ketterson AA, Masselink WT, Gedymin JS, Klem J, Peng CK, Kopp WF, et al. Characterization of InGaAs/AlGaAs pseudomorphic modulation-doped field effect transistor. IEEE Trans Electron Devices 1986;33:564–71.
[3] Shawki T, Salmer G, El-Sayed O. MODFET 2-D hydrodynamic energy modeling: optimization of subquarter-micron-gate structures. IEEE Trans Electron Devices 1990;37:21–30.
[4] Delemer JD, Rousseau M, De Jaeger JC, Lefebvre M. Recent improvements of 2-D hydrodynamic model for HEMT simulations. In: 10th III–V Semiconductor device simulation workshop, 1997.
[5] Lush GB, Melloch MR, Lundstrom MS. Hole lifetimes in n-type GaAs. Emis data reviews series no. 16, p. 139 [INSPEC publication].
[6] Chau HF, Pavlidis D. A physics-based fitting and extrapolation method for measured impact ionisation coefficients in III–V semiconductors. J Appl Phys 1992;72(2):531–8.
[7] Vanbésien O. Ionisation par choc dans le GaAs, l'Al_x $Ga_{1-x}As$ et dans les hétérostructures à multipuits quantiques. Mémoire de DEA. Lille, 1987.
[8] Baccarani G, Wordeman MR. An investigation of steady-state velocity overshoot in silicon. Solid-State Electron 1985;28(4):407–16.
[9] Delemer JD. Elaboration d'un nouveau modèle hydrodynamique bidimensionnel de transistor à effet de champ à hétérojonctions pour l'amplification de puissance en millimétrique. PhD thesis. Lille, 2000.
[10] Jacobini C, Reggiani L. The Monte Carlo method for the solution of charge transport in semiconductors with applications to covalent materials. Rev Mod Phys 1983;55(3):645–705.
[11] Ibrahim M. Two-dimensional simulation of microwave GaAs submicronic-gate FETs. PhD thesis. Cairo University, 1983.
[12] Van der Vorst HA. Bi-CGSTAB: fast and smoothly nonsymmetric linear systems. J Sci Stat Comput 1992;12:631–44.
[13] Nougier JP. Méthode de calcul numérique. Paris: MASSON; 1985.
[14] Hédoire J. Simulation hydrodynamique bidimensionnelle de transistors de type HEMT pseudomorphique. Analyse physique et optimisation pour l'amplification de puissance hyperfréquence. PhD thesis, Lille, 1997.
[15] Wada Y, Tomizawa M. Drain avalanche breakdown in gallium arsenide MESFET's. IEEE Trans Electron Devices 1988;35(11):1765–70.
[16] Lee JL, Kim H, Mun JK, Maeng SJ. A Ku-band T-shapped GaAs power MESFET with high breakdown voltage for satellite communications. IEEE Electron Device Lett 1988;19(7):250–2.
[17] Gaquiere C, Bonte B, Theron D, Crosnier Y, Arsene-Henri P, Pacou T. Breakdown analysis of an asymmetrical double recessed power MESFET's. IEEE Trans Electron Devices 1995;42(2):209–14.

[18] Lu SS, Meng CC, Lin YS, Lan H. The effect of gate recess profile on device performance of $Ga_{0.51}In_{0.49}P/In_{0.2}Ga_{0.8}As$ doped-channel FET's. IEEE Trans Electron Devices 1999;46(1):48–54.

[19] Huang JC et al. A double-recessed $Al_{0.24}GaAs/In_{0.16}GAs$ pseudomorphic HEMT for Ka- and Q-band power application. IEEE Electron Devices 1993;41(5):752–9.